

Generation of broadband polarization-orthogonal photon pairs via the dispersion-engineered thin-film lithium niobate waveguide

Ji-Ning Zhang(张继宁), Tong-Yu Zhang(张同宇), Jia-Chen Duan(端家晨), Yan-Xiao Gong(龚彦晓), and Shi-Ning Zhu(祝世宁)

Citation: Chin. Phys. B, 2024, 33 (**11**): 110301. DOI: 10.1088/1674-1056/ad757c
Journal homepage: http://cpb.iphy.ac.cn; http://iopscience.iop.org/cpb

What follows is a list of articles you may be interested in

Compact generation scheme of path-frequency hyperentangled photons using 2D periodical nonlinear photonic crystal

Yang-He Chen(陈洋河), Bo Ji(季波), Nian-Qin Li(李念芹), Zhen Jiang(姜震), Wei Li(李维),Yu-Dong Li(李昱东), Liang-Sen Feng(冯梁森), Teng-Fei Wu(武腾飞), and Guang-Qiang He(何广强)
Chin. Phys. B, 2023, 32 (**12**): 120307. DOI: 10.1088/1674-1056/ad0625

Generation of hyperentangled photon pairs based on lithium niobate waveguide

Yang-He Chen(陈洋河), Zhen Jiang(姜震), and Guang-Qiang He(何广强)
Chin. Phys. B, 2023, 32 (**9**): 090306. DOI: 10.1088/1674-1056/acd5c4

Effect of thickness variations of lithium niobate on insulator waveguide on the frequency spectrum of spontaneous parametric down-conversion

Guang-Tai Xue(薛广太), Xiao-Hui Tian(田晓慧), Chi Zhang(张弛), Zhenda Xie(谢臻达), Ping Xu(徐平), Yan-Xiao Gong(龚彦晓), and Shi-Ning Zhu(祝世宁)
Chin. Phys. B, 2021, 30 (**11**): 110313. DOI: 10.1088/1674-1056/ac22a1

Widely tunable single-photon source with high spectral-purity from telecom wavelength to mid-infrared wavelength based on MgO:PPLN

Chang-Wei Sun(孙昌伟), Yu Sun(孙宇), Jia-Chen Duan(端家晨), Guang-Tai Xue(薛广太), Yi-Chen Liu(刘奕辰), Liang-Liang Lu(陆亮亮), Qun-Yong Zhang(张群永), Yan-Xiao Gong(龚彦晓), Ping Xu(徐平), and Shi-Ning Zhu(祝世宁)
Chin. Phys. B, 2021, 30 (**10**): 100312. DOI: 10.1088/1674-1056/ac20cb

Improving the purity of heralded single-photon sources through spontaneous parametric down-conversion process

Jing Wang(王静), Chun-Hui Zhang(张春辉), Jing-Yang Liu(刘靖阳), Xue-Rui Qian(钱雪瑞), Jian Li(李剑), and Qin Wang(王琴)
Chin. Phys. B, 2021, 30 (**7**): 070304. DOI: 10.1088/1674-1056/abfb5c

---

SPECIAL TOPIC — Quantum communication and quantum network

Generation of broadband polarization-orthogonal photon pairs via the dispersion-engineered thin-film lithium niobate waveguide

Ji-Ning Zhang(张继宁), Tong-Yu Zhang(张同宇), Jia-Chen Duan(端家晨), Yan-Xiao Gong(龚彦晓)†, and Shi-Ning Zhu(祝世宁)

National Laboratory of Solid State Microstructures, School of Physics, Nanjing University, Nanjing 210093, *China*

(Received 9 August 2024; revised manuscript received 29 August 2024; accepted manuscript online 30 August 2024)

Broadband photon pairs are highly desirable for quantum metrology, quantum sensing, and quantum communication. Such sources are usually designed through type-0 phase-matching spontaneous parametric down-conversion (SPDC) that makes the photon pairs hard to separate in the frequency-degenerate case and thus limits their applications. In this paper, we design a broadband frequency-degenerate telecom-band photon pair source via the type-II SPDC in a dispersion-engineered thin-film lithium niobate waveguide, where the polarization modes of photon pairs are orthogonal and thus are easily separated deterministically. With a 5-mm-long waveguide, our design can achieve a bandwidth of 5.56 THz (44.8 nm), which is 8.6 times larger than that of the bulk lithium niobate, and the central wavelength can be flexibly adjusted. Our design is a promising approach towards high-quality integrated photon sources and may have wide applications in photonic quantum technologies.

Keywords: broadband photon pair source, spontaneous parametric down-conversion, dispersion engineering, thin-film lithium niobate waveguide

PACS: 03.67.–a, 42.50.–p, 42.65.–k, 42.82.–m **DOI:** 10.1088/1674-1056/ad757c

1. Introduction

Photon pairs are a basic resource for quantum photonic technologies, which have been developed rapidly in recent years. In particular, broadband photon pairs add significant advantages to a variety of quantum photonic applications. On the one hand, the high information capacity of broadband photons can provide abundant resources for high-dimensional quantum communication networks.[1,2] On the other hand, their short correlation time allows for enhancing sensitivity and resolution in quantum metrology tasks,[3–5] such as quantum optical coherence tomography,[6] lithography,[7,8] spectroscopy,[9] and clock synchronization.[10,11]

The technique of type-0 phase-matching spontaneous parametric down-conversion (SPDC) is a widely used method for producing bright and broadband photon pairs.[12–16] However, the photon pairs have the same polarization modes, making it challenging to separate them in the case of frequency-degenerate case. This limitation restricts their utilization in many quantum information tasks requiring frequency-degenerate photons, such as quantum coherence tomography and quantum interferometric lithography. Non-collinear type-I SPDC source can provide broadband, separated frequency-degenerate photon pairs.[17,18] However, the non-collinear phase matching limits the interaction length and photon collecting fraction, and hence is usually subjected to low efficiency. In contrast, the type-II SPDC can generate photon pairs with orthogonal polarization modes, thus allowing for the deterministic separation of the two photons through the polarization beam splitter in a simple and effective way. But unfortunately, the natural spectral bandwidth is rather narrow in type-II SPDC due to the different dispersion properties of orthogonally-polarized photon pairs.[19] To broaden the bandwidth, Fraine *et al*. employed the technique of chirped quasi-phase matching (QPM) and obtained a bandwidth of $\sim$ 125 nm.[20] However, the chirped photon pairs are usually not transform-limited, requiring phase correction. On the other hand, Shimizu and Edamatsu utilized periodically-poled MgO-doped stoichiometric $LiTaO_3$ to produce broadband photon pairs due to the weak birefringence of the crystal.[21] However, the type-II effective nonlinear coefficient of the crystal is too small which may limit its generation efficiency.

In this paper, we propose a scheme for generating broadband and bright type-II SPDC photon pairs based on thin-film lithium niobate (TFLN) waveguide. Recently, the TFLN platform has shown its high performance in integrated optics[22,23] due to the low optical transmission loss, large electro-optical and second-order nonlinear coefficients, and strong mode confinement. In particular, the dispersion engineering of the TFLN waveguides has been extensively explored in broadening the bandwidth of second harmonic generation,[24] optical parametric amplification,[25–27] and type-0 SPDC processes.[15,16,28] Here, by introducing dispersion engineering, we design a ridge waveguide that sat-

†Corresponding author. E-mail: gongyanxiao@nju.edu.cn

© 2024 Chinese Physical Society and IOP Publishing Ltd

isfies the dispersion condition required for broadband type-II SPDC. Simulation calculations show that our design enables a spectral bandwidth of 5.56 THz (44.8 nm) with a 5-mm-long waveguide, and a spectral brightness of 1.51×10^7 Hz/(nm·mW).

2. Theoretical model

For a degenerate type-II SPDC pumped by a continuous-wave (cw, coherent time ≥ 1 μs) laser of angular frequency ω_p, the generated two-photon state is characterized as

$$|\psi\rangle = A\int \mathrm{d}\nu\,\phi(\Delta k)|\omega_0+\nu\rangle_\mathrm{s}|\omega_0-\nu\rangle_\mathrm{i}, \tag{1}$$

where $\omega_0=\omega_\mathrm{p}/2$ is the central frequency of signal (s) and idler (i) photons spectrum, with ν denoting the frequency detuning. The coefficient A absorbs all the constants and is a slowly varying function of frequency, which is given in Section 5 for details. The complex function $\phi(\Delta k)$ is the photon pair spectral amplitude, given by

$$\phi(\Delta k)=\mathrm{sinc}\left(\frac{\Delta kL}{2}\right)\exp\left(-\mathrm{i}\frac{\Delta kL}{2}\right), \tag{2}$$

where L is the crystal length, and the joint spectral intensity is then given by

$$P=\mathrm{sinc}^2(\Delta kL/2). \tag{3}$$

For QPM, the phase mismatch Δk is given by

$$\Delta k = k_\mathrm{p}(\omega_\mathrm{p})-k_\mathrm{s}(\omega_\mathrm{s})-k_\mathrm{i}(\omega_\mathrm{i})-\frac{2\pi}{\Lambda}, \tag{4}$$

where Λ is the poling period. The wave vectors of signal and idler photons can be respectively expanded around frequency ω_0 as

$$\begin{aligned} k_\mathrm{s}(\omega_\mathrm{s}) &= k_\mathrm{s}(\omega_0)+\sum_{m=1}^{\infty}\frac{\beta_m^\mathrm{s}}{m!}\nu^m,\\ k_\mathrm{i}(\omega_\mathrm{i}) &= k_\mathrm{i}(\omega_0)+\sum_{m=1}^{\infty}\frac{\beta_m^\mathrm{i}}{m!}(-\nu)^m, \end{aligned} \tag{5}$$

where $\beta_m^{\mathrm{s(i)}}=\mathrm{d}^m k_\mathrm{s(i)}/\mathrm{d}\,\omega_\mathrm{s(i)}^m|_{\omega_\mathrm{s(i)}=\omega_0}$ is m^th-order dispersion. Thus, Δk can be derived as

$$\begin{aligned} \Delta k \;=\; & k_\mathrm{p}(\omega_\mathrm{p})-k_\mathrm{s}(\omega_0)-k_\mathrm{i}(\omega_0)-\frac{2\pi}{\Lambda}\\ & -\sum_{m=1}^{\infty}\left[\frac{\beta_m^\mathrm{s}\nu^m+\beta_m^\mathrm{i}(-\nu)^m}{m!}\right]. \end{aligned} \tag{6}$$

The poling period Λ can be explicitly calculated to satisfy the QPM condition, namely,

$$k_\mathrm{p}(\omega_\mathrm{p})-k_\mathrm{s}(\omega_0)-k_\mathrm{i}(\omega_0)-2\pi/\Lambda=0. \tag{7}$$

Then, in order to maximize the bandwidth of the photon pair spectrum $\phi(\Delta k)$, Δk should be minimized around the detuning ν. Hence, we have the following conditions:

$$|\beta_m^\mathrm{s}-\beta_m^\mathrm{i}|=0\ \ (m=2n-1),\ \ |\beta_m^\mathrm{s}+\beta_m^\mathrm{i}|=0\ \ (m=2n), \tag{8}$$

where $n\in\mathbb{N}^+$. For type-II phase matching case, we can only consider the dominant term of $m=1$, and minimize it, namely,

$$|\beta_1^\mathrm{s}-\beta_1^\mathrm{i}|=0. \tag{9}$$

Recalling $\beta_1=1/v_\mathrm{g}=n_\mathrm{g}/c$, with v_g and n_g denoting the group velocity and group index, respectively, Eq. (9) can be reduced to $n_\mathrm{g}^\mathrm{s}=n_\mathrm{g}^\mathrm{i}$, which is referred to as group index matching condition. Under this condition, the phase-matching bandwidth can be significantly broadened, and then limited by group-velocity dispersion (GVD) and higher-order dispersion. According to the term $m=2$ in Eq. (8), we get the phase mismatch $\Delta k\approx D\nu^2$ with the dispersion factor $D=(\beta_2^\mathrm{s}+\beta_2^\mathrm{i})/2$.

3. Waveguide design

We design a TFLN waveguide structure that satisfies both the type-II phase matching condition and the group index matching condition in telecom band given by Eqs. (7) and (9), respectively, where the pump, signal, and idler light fields are in quasi-TM_{00}, quasi-TE_{00}, and quasi-TM_{00} modes, respectively. The optimized cross section of the designed X-cut TFLN waveguide is depicted in Fig. 1(a), where the lithium niobate film with a thickness of $h_2=350$ nm is etched on and also clad with 2-μm-thick silica. The top width of the waveguide is $w=1020$ nm, with a sidewall angle of $\theta=65°$, and the etching depth is $h_1=250$ nm.

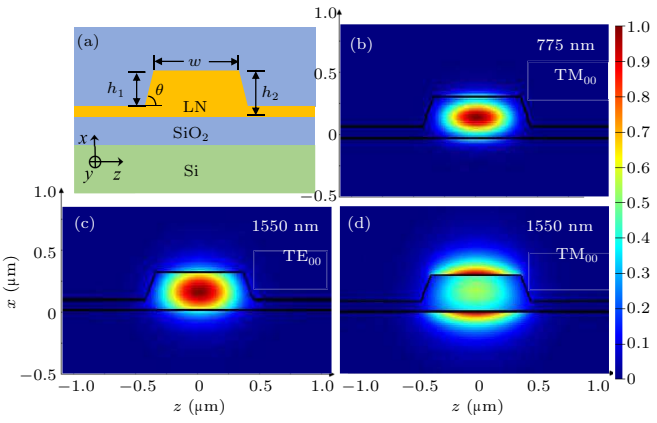


Fig. 1. (a) Cross section of the TFLN waveguide structure, where the ridge waveguide is located on $h_2=350$ nm thick X-cut LNOI wafer, with the top width of $w=1020$ nm, the sidewall angle of $\theta=65°$, and the etching depth of $h_1=250$ nm. (b)–(d) Field distributions of the pump, signal and idler modes.

The field distributions of pump, signal and idler modes are simulated as shown in Figs. 1(b)–1(d) by utilizing the Mode Solutions v8.6 software, with the material dispersion of lithium niobate given by Ref. [29]. It can be seen that the

TM_{00} mode is more confined than the TE_{00} mode with some field entering the silica layers. The corresponding group index curves of the TE_{00} and TM_{00} modes are plotted in Fig. 2. The group index matching condition is fulfilled at the intersection 1550 nm.

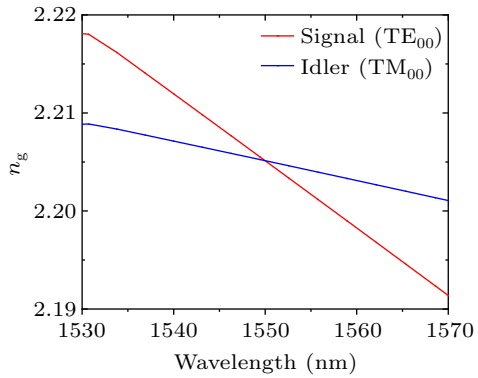


Fig. 2. Group index curves of signal and idler photons in the designed waveguide.

4. Spectra and bandwidths

Then taking 1550 nm as the central wavelength of signal and idler photons, we can calculate the poling period as $\Lambda = 2.09$ μm. Next, by setting waveguide length $L = 5$ mm, we calculate the phase mismatching $\Delta kL/2\pi$ as shown in Fig. 3(a) where we can infer the largest phase-matching bandwidth to be 12.8 THz. We plot the two-photon spectrum intensity in Fig. 3(b), with the comparison against that of bulk lithium niobate crystal of the same length. We can see that the bandwidth, defined as full width at half maximum, is 44.8 nm (1527.5 nm–1572.3 nm), corresponding to a frequency bandwidth of 5.56 THz, which is 8.6 times larger than the 0.65 THz bandwidth using the bulk lithium niobate crystal. We can further calculate the bandwidth–length product $\Delta\lambda L$ as 22.40 μm^2.

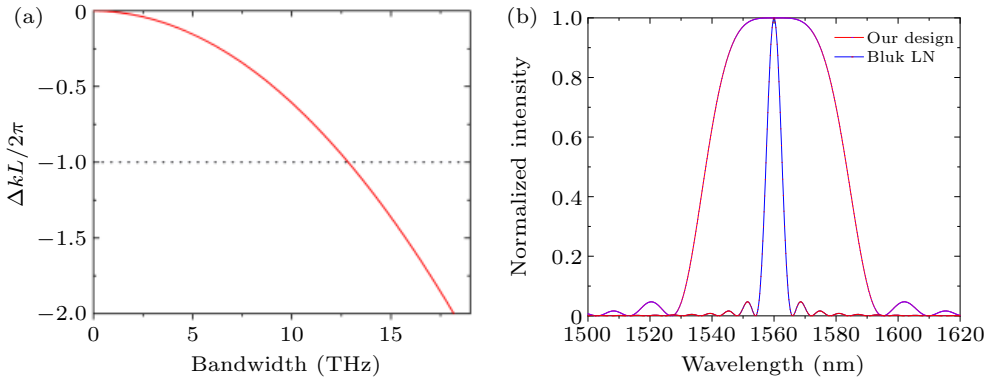


Fig. 3. (a) The phase mismatching $\Delta kL/2\pi$. Dashed line indicates the point where the phase-mismatch sinc function reaches zero. (b) Simulated normalized two-photon spectrum intensities of our design (red line) and bulk lithium niobate crystal (blue line).

5. Brightness

Considering a cw laser with power P as the pump and following analogy calculations made in Refs. [30–32], we can write the constant A in Eq. (1) as

$$A = \mathrm{i}L\sqrt{\frac{P\omega_0^2 d_{\mathrm{eff}}^2 \zeta^2}{2\varepsilon_0 c^3 n_{\mathrm{p}} n_{\mathrm{s0}} n_{\mathrm{i0}} S}}, \tag{10}$$

where $d_{\mathrm{eff}} = 2d_{31}/\pi \approx 1.78$ pm/V is the effective nonlinear coefficient for type-II SPDC, with n_j $(j = \mathrm{p}, \mathrm{s0}, \mathrm{i0})$ representing the refractive index of pump, signal, and idler photons at their central wavelengths, respectively. The parameter $S = (S_{\mathrm{p}} S_{\mathrm{s0}} S_{\mathrm{i0}})^{1/3}$ is the effective mode area, with S_j $(j = \mathrm{p}, \mathrm{s0}, \mathrm{i0})$ given by

$$S_j = \frac{\left(\int_{\mathrm{all}} |\boldsymbol{E}_j|^2 \mathrm{d}x\mathrm{d}z\right)^3}{\left|\int_{\chi^{(2)}} |\boldsymbol{E}_j|^2 \boldsymbol{E}_j \mathrm{d}x\mathrm{d}z\right|^2}, \tag{11}$$

and $\boldsymbol{E}_j$ $(j = \mathrm{p}, \mathrm{s0}, \mathrm{i0})$ denoting the electric fields of the pump, signal, and idler photons, respectively. The parameter ζ represents the spatial mode overlap factor between the pump, signal, and idler modes, given by

$$\zeta = \frac{\int_{\chi^{(2)}} E_{\mathrm{p},z} E^*_{\mathrm{s0},x} E_{\mathrm{i0},z} \mathrm{d}x\mathrm{d}z}{\left(\left|\int_{\chi^{(2)}} |\boldsymbol{E}_{\mathrm{p}}|^2 \boldsymbol{E}_{\mathrm{p}} \mathrm{d}x\mathrm{d}z\right| \left|\int_{\chi^{(2)}} |\boldsymbol{E}_{\mathrm{s0}}|^2 \boldsymbol{E}_{\mathrm{s0}} \mathrm{d}x\mathrm{d}z\right| \left|\int_{\chi^{(2)}} |\boldsymbol{E}_{\mathrm{i0}}|^2 \boldsymbol{E}_{\mathrm{i0}} \mathrm{d}x\mathrm{d}z\right|\right)^{\frac{1}{3}}}, \tag{12}$$

where $\int_{\mathrm{all}}$ and $\int_{\chi^{(2)}}$ represent integrations over all space and the lithium niobate layer, respectively.

Then we can obtain the photon pair generation rate as follows:

$$R = \langle\psi|\psi\rangle = |A|^2 \int \mathrm{d}\nu |\phi(\nu)|^2. \tag{13}$$

By substituting Eqs. (2), (10)–(12), and the group index matching condition of $n_g^i = n_g^s$ into Eq. (13), we have

$$R = \frac{2\sqrt{2}\pi^{\frac{1}{2}} P L^{\frac{3}{2}} \omega_0^2 d_{\text{eff}}^2 \zeta^2}{3\varepsilon_0 c^3 n_p n_{s0} n_{i0} S |D|^{\frac{1}{2}}}. \tag{14}$$

As shown in Table 1, we calculate the values of each parameter in Eq. (14) in our design. Supposing that $L = 5$ mm and $P = 1$ mW, we can estimate the generation rate to be 6.76×10^8 Hz, with the corresponding spectral brightness of 1.51×10^7 Hz/(nm·mW).

Table 1. List of parameters.

Variable	Parameter	Simulation value
S	effective mode area	2.151 μm^2
ζ	spatial mode overlap factor	0.866
D	dispersion factor	1.826 ps^2/m
n_p	refractive index of pump at ω_p	2.041
n_{s0}	refractive index of signal at ω_0	1.759
n_{i0}	refractive index of idler at ω_0	1.654

6. Discussion

We now discuss the experimental feasibility of our design. The waveguide structure and poling period are experimentally feasible with current TFLN techniques.[15,25,26,33,34] Moreover, our scheme is tolerant to the waveguide fabrication deviations. Firstly, we consider the deviation in waveguide width w and etching depth h_2 and show the simulation results of dispersion in Fig. 4(a). As shown in dashed line, when w changes to $w_1 = 1000$ nm and $w_2 = 1040$ nm, the intersection point of group indices n_g of signal and idler photons changes from 1550 nm to 1548.2 nm and 1552.8 nm, respectively, and the bandwidth changes to 5.544 THz and 5.573 THz, respectively. The deviation in h_1 has more influence on the dispersion of TM_{00}, as shown in solid line. When h_1 changes to $h_1^1 = 230$ nm and $h_1^2 = 270$ nm, the intersection wavelength changes to 1555.6 nm and 1544.7 nm, respectively, and the bandwidth changes to 5.541 THz and 5.584 THz, respectively. The group index matching condition can still be satisfied at slightly deviated wavelengths, and the change of bandwidth is quite small, which can be neglected in these conditions, and thus we can still obtain broadband photon pairs by finely tuning the pump wavelength and poling period.

Secondly, we further plot the group index matching wavelength as a function of lithium niobate film thickness h_2 in Fig. 4(b) with the blue dotted line. It can be seen that the influence of film thickness variation is more obvious than waveguide width and etching depth, as the TM_{00} field is strongly compressed in our design and its dispersion is more sensitive to thickness variation compared with the other geometric structure parameters.

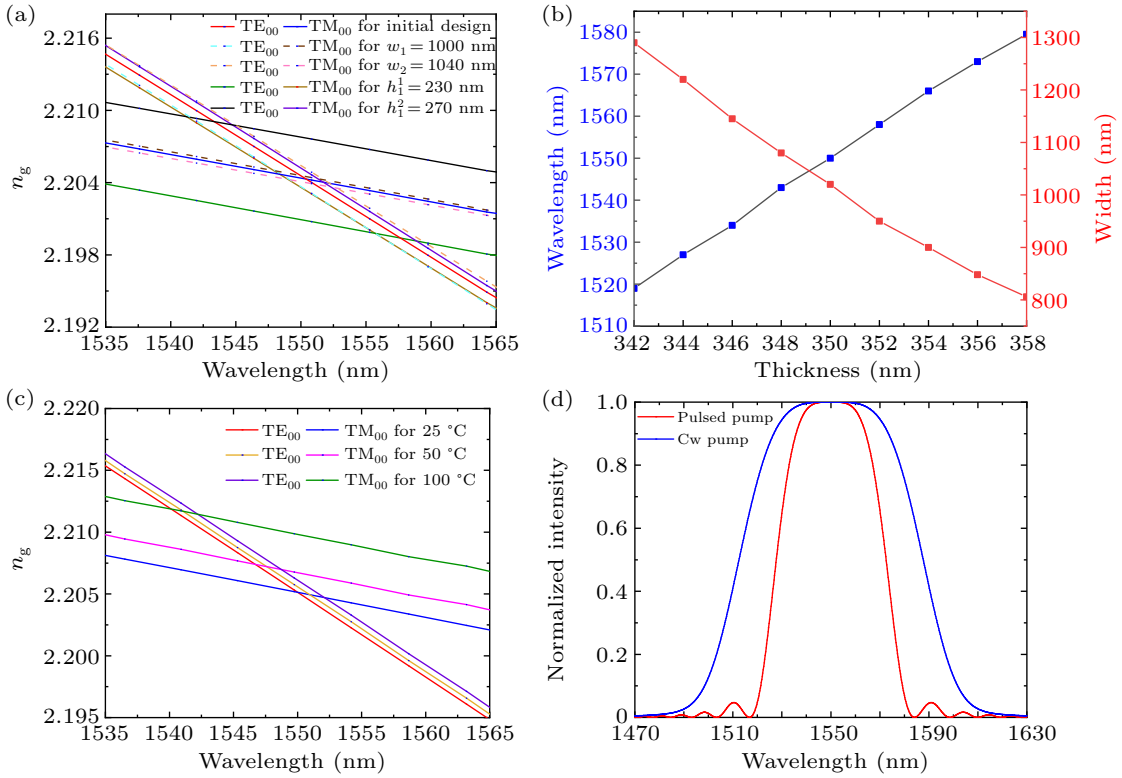


Fig. 4. Simulation of the influence of fabrication deviations, operating temperature shifts and pump bandwidth variation. (a) The group indices of the TM_{00} and TE_{00} modes in the case of deviations in waveguide width and etch depth. (b) The wavelength (blue dotted line) satisfying the group index matching condition and the corresponding waveguide width (red dotted line) required to generate 1550 nm degenerate photon pairs against lithium niobate film thickness. (c) The group indices of the TM_{00} and TE_{00} modes at different waveguide temperatures. (d) Simulated normalized two-photon spectrum intensities with cw pump (red line) and pulsed pump (blue line).

If the shifted degenerate wavelength does not fit our application scenario, we could measure the film thickness h_2 before fabrication and change other geometric parameters based on h_2. As shown by the red dotted line in Fig. 4(b), the degenerate wavelengths can be adjusted to 1550 nm under different film thickness by varying the waveguide top width w, and the poling period should be adjusted as well. For example, when the film thickness is 344 nm, we can get 1550-nm-degenerate photon pairs by adjusting the waveguide width to $w = 1220$ nm. In addition, the group indices of signal and idler are temperature dependent and can therefore be fine tuned by choosing an appropriate operating temperature. As shown in Fig. 4(c), when the waveguide temperature rises to 50 °C and 100 °C, the intersection point of group indices of signal and idler photons changes from 1550 nm to 1547.5 nm and 1541.1 nm, respectively. The above analysis results also reflect the tunability of our design on waveguide width, etching depth, film thickness and temperature. We can flexibly adjust the geometric parameters and operating temperature to obtain the broadband photon pair source at user-chosen target wavelengths.

Furthermore, the spectral properties of pump could affect two-photon bandwidths. In the case of the broadband pulsed pump, the generated two-photon state changes to[35]

$$|\psi\rangle \propto \int \mathrm{d}\omega_\mathrm{s}\,\mathrm{d}\omega_\mathrm{i}\,\alpha(\omega_\mathrm{s}+\omega_\mathrm{i})\phi(\Delta k)|\omega_\mathrm{s}\rangle_\mathrm{s}|\omega_\mathrm{i}\rangle_\mathrm{i}, \qquad (15)$$

where $\alpha(\omega_\mathrm{s}+\omega_\mathrm{i})$ is the pump envelope function. We plot the normalized two-photon spectrum intensities when the coherent time of pump light is 1 ps with a Gaussian-distribution in Fig. 4(d) (blue line), where the two-photon bandwidth is extended to 75.0 nm, which is much broader compared to the case where the pump light is cw (red line). Therefore, the pump function could significantly affect the two-photon spectral distribution and we can increase the two-photon bandwidth by increasing the pump bandwidth.

7. Conclusion

In summary, we designed a periodically-poled TFLN waveguide for producing broadband frequency-degenerate polarization-orthogonal photon pairs by employing the type-II phase-matching SPDC. In contrast to the previous broadband sources based on the type-0 SPDC, the photon pairs can be separated deterministically more easily. The waveguide structure is designed to make the group index curves of the TE_{00} and TM_{00} modes crossing at 1550 nm, enabling the bandwidth of photon pairs to be increased. Our simulation results show that the bandwidth of our source is 5.56 THz (44.8 nm) with the bandwidth–length product of 22.85 $\mu\mathrm{m}^2$, which is 8.6 times larger than that of the bulk lithium niobate. The theoretical brightness of our source is calculated to be 1.51×10^7 Hz/(nm·mW). Additionally, our design is experimentally feasible and highly tolerant to waveguide fabrication deviations. Furthermore, we can further expand the bandwidth by combining with other methods such as chirping quasi-phase matching[36] and temperature gradient methods.[37] We envision that our approach will motivate efforts to develop integrated nanophotonics for a variety of applications in quantum technologies.

Acknowledgments

Project supported by the National Key Research and Development Program of China (Grant No. 2019YFA0705000), Innovation Program for Quantum Science and Technology (Grant No. 2021ZD0301500), Leading-edge Technology Program of Jiangsu Natural Science Foundation (Grant No. BK20192001), and the National Natural Science Foundation of China (Grant Nos. 51890861 and 11974178).

References

[1] Wengerowsky S, Joshi S K, Steinlechner F, Hübler H and Ursin R 2018 *Nature* **564** 225
[2] Joshi S K, Aktas D, Wengerowsky S, Lončarić M, Neumann S P, Liu B, Scheidl T, Lorenzo G C, Samec Z, Kling L, Qiu A, Razavi M, Stipčević M, Rarity J and Ursin R 2020 *Sci. Adv.* **6** eaba0959
[3] Giovannetti V, Lloyd S and Maccone L 2011 *Nat. Photon.* **5** 222
[4] Chen Y, Hong L and Chen L 2022 *Front. Phys.* **10** 892519
[5] Katamadze K, Pashchenko A, Romanova A and Kulik S 2022 *JETP Lett.* **115** 581
[6] Abouraddy A F, Nasr M B, Saleh B E A, Sergienko A V and Teich M C 2002 *Phys. Rev. A* **65** 053817
[7] Boto A N, Kok P, Abrams D S, Braunstein S L, Williams C P and Dowling J P 2000 *Phys. Rev. Lett.* **85** 2733
[8] D'Angelo M, Chekhova M V and Shih Y 2001 *Phys. Rev. Lett.* **87** 013602
[9] Saleh B E A, Jost B M, Fei H B and Teich M C 1998 *Phys. Rev. Lett.* **80** 3483
[10] Giovannetti V, Lloyd S and Maccone L 2004 *Science* **306** 1330
[11] Quan R, Dong R, Zhai Y, Hou F, Xiang X, Zhou H, Lv C, Wang Z, You L, Liu T and Zhang S 2019 *Opt. Lett.* **80** 3483
[12] Tanzilli S, De Riedmatten H, Tittel W, Zbinden H, Baldi P, De Micheli M, Ostrowsky D B and Gisin N 2001 *Electron. Lett.* **37** 26
[13] Dayan B, Pe'er A, Friesem A A and Silberberg Y 2005 *Phys. Rev. Lett.* **94** 043602
[14] Nasr M B, Carrasco S, Saleh B E A, Sergienko A V, Teich M C, Torres J P, Torner L, Hum D S and Fejer M M 2008 *Phys. Rev. Lett.* **100** 199903
[15] Javid U A, Ling J, Staffa J, Li M, He Y and Lin Q 2021 *Phys. Rev. Lett.* **127** 183601
[16] Fang X X, Wang L and Lu H 2024 *Opt. Express* **32** 22945
[17] Carrasco S, Nasr M B, Sergienko A V, Saleh B E A, Teich M C, Torres J P and Torner L 2006 *Opt. Lett.* **31** 253
[18] Okano M, Okamoto R, Tanaka A, Subashchandran S and Takeuchi S 2012 *Opt. Express* **20** 13977
[19] Rubin M H, Klyshko D N, Shih Y H and Sergienko A V 1994 *Phys. Rev. A* **50** 5122
[20] Fraine A, Minaeva O, Simon D, Egorov R and Sergienko A 2012 *Opt. Lett.* **37** 1910
[21] Shimizu R and Edamatsu K 2009 *Opt. Express* **17** 16385
[22] Saravi S, Pertsch T and Setzpfandt F 2021 *Adv. Opt. Mater.* **9** 2100789
[23] Vazimali M G and Fathpour S 2022 *Adv. Photon.* **4** 034001
[24] Jankowski M, Langrock C, Desiatov B, Marandi A, Wang C, Zhang M, Phillips C R, Lončar M and Fejer M M 2020 *Optica* **7** 40
[25] Jankowski M, Jornod N, Langrock C, Desiatov B, Marandi A, Lončar M and Fejer M M 2022 *Optica* **9** 273
[26] Ledezma L, Sekine R, Guo Q, Nehra R, Jahani S and Marandi A 2022 *Optica* **9** 303

[27] Hwang A Y, Stokowski H S, Park T, Jankowski M, McKenna T P, Langrock C, Mishra J, Ansari V, Fejer M M and Safavi-Naeini A H 2023 *Optica* **10** 1535

[28] Xue G T, Niu Y F, Liu X, Duan J C, Chen W, Pan Y, Jia K, Wang X, Liu H Y, Zhang Y, Xu P, Zhao G, Cai X, Gong Y X, Hu X, Xie Z and Zhu S 2021 *Phys. Rev. Appl.* **15** 064059

[29] Zelmon D E, Small D L and Jundt D 1997 *J. Opt. Soc. Am. B* **14** 3319

[30] Yang Z, Liscidini M and Sipe J E 2008 *Phys. Rev. A* **77** 033808

[31] Luo R, He Y, Liang H, Li M and Lin Q 2018 *Optica* **5** 1006

[32] Duan J C, Zhang J N, Zhu Y J, Sun C W, Liu Y C, Xu P, Xie Z, Gong Y X and Zhu S N 2020 *J. Opt. Soc. Am. B* **37** 2139

[33] Wang C, Langrock C, Marandi A, Jankowski M, Zhang M, Desiatov B, Fejer M M and Lončar M 2018 *Optica* **5** 1438

[34] Zhao J, Ma C, Rüsing M and Mookherjea S 2020 *Phys. Rev. Lett.* **124** 163603

[35] Wei B, Cai W H, Ding C, Deng G W, Shimizu R, Zhou Q and Jin R B 2021 *Opt. Express* **29** 256

[36] Sensarn S, Yin G Y and Harris S E 2010 *Phys. Rev. Lett.* **104** 253602

[37] Katamadze K and Kulik S 2011 *J. Exp. Theor. Phys.* **112** 20